AGU100 ADVANCING EARTH AND SPACE SCIENCE

JGR

Journal of Geophysical Research: Atmospheres

RESEARCH ARTICLE
10.1029/2018JD028315

Key Points:
- Ambient water vapor supersaturation can be calculated using aerosol and cloud measurements
- Low supersaturations less than 0.05% were found for a dense radiation fog in the North China Plain
- Significant contribution of unactivated haze particles to the total fog droplets was found in the heavily polluted fog episode

Correspondence to:
C. Zhao,
zcs@pku.edu.cn

Citation:
Shen, C., Zhao, C., Ma, N., Tao, J., Zhao, G., Yu, Y., & Kuang, Y. (2018). Method to estimate water vapor supersaturation in the ambient activation process using aerosol and droplet measurement data. *Journal of Geophysical Research: Atmospheres*, *123*, 10,606–10,619. https://doi.org/10.1029/2018JD028315

Received 12 JAN 2018
Accepted 26 JUL 2018
Accepted article online 5 AUG 2018
Published online 28 SEP 2018

Method to Estimate Water Vapor Supersaturation in the Ambient Activation Process Using Aerosol and Droplet Measurement Data

Chuanyang Shen[1], Chunsheng Zhao[1], Nan Ma[2], Jiangchuan Tao[2], Gang Zhao[1], Yingli Yu[1], and Ye Kuang[2]

[1]Department of Atmospheric and Oceanic Sciences, School of Physics, Peking University, Beijing, China, [2]Institute for Environmental and Climate Research, Jinan University, Guangzhou, China

Abstract Water vapor supersaturation, as one of the most important environmental parameters during the formation of clouds or fogs, cannot be directly measured, and few studies have been carried out to estimate it in the ambient activation process. In this study, a new method to estimate the water vapor supersaturation based on the inverse application of κ-Köhler theory is proposed. Aerosol hygroscopic parameter κ, dry particle size distributions, and wet droplet size distributions were employed and a comparison of predicted droplet number concentration with the measurement results was made to obtain the effective supersaturation during the activation process. Using this method, we acquired the supersaturations varying from 0.01% to 0.05% in a fog episode observed in the North China Plain. In this fog episode, both hydrated unactivated droplets and activated droplets play a part in the total detected droplet number concentrations with the unactivated droplets' ratio decreasing with size. The sensitivity study was also made to evaluate the effects of droplet and aerosol hygroscopic measurement errors on the supersaturation ratio estimation. Water vapor supersaturation obtained with this method can be regarded as an effective value and can be further applied to cloud analysis in the future. This method is only based on conventional measurements of aerosol and droplets and does not rely on any other data, which makes it flexible and easy to perform. Calculated supersaturations and critical diameters can also deepen the understanding of ambient activation process and corresponding interactions between aerosol and droplet characteristics.

1. Introduction

Clouds and fogs are two typical ambient activation processes, and their evolution not only affect human life but also play a vital role in Earth's climate through aerosol direct and indirect effects (Ackerman et al., 2004; Guo et al., 2017; Kiehl & Briegleb, 1993). Previous studies have shown that these activation processes can only happen under water vapor supersaturation except some special cases (Kulmala et al., 1997). Water vapor supersaturation is defined as the state that the water vapor partial pressure in the air is greater than the saturated vapor partial pressure with respect to liquid or ice, respectively. The relationship between the water vapor supersaturation and microphysical characteristics of clouds or fogs is one of the key issues in theoretical and applied physics of clouds. The supersaturation inside clouds is also important for mesoscale and climate models as it is closely associated with the cloud condensation nuclei (CCN) which is one of the most important parameters in the clouds (Cheng et al., 2007).

However, currently, there is no widely accepted and reliable method to measure the supersaturation accurately while minor errors in supersaturation can lead to great differences to the activation characteristics. In convective-type clouds, supersaturations are of the order of 1%, while layer-type clouds typically have a much lower supersaturation (Hudson, 1980), so the measurement of this parameter requires high accuracy of the instrument. In addition, it is not possible to substantiate the accuracy near saturation of the hygrometer by comparing it against the National Bureau of Standards (NBS) standard humidity generator, whose upper limit is 98% ± 0.2% relative humidity (Hasegawa & Little, 1977). Conventional hygrometers cannot measure saturation ratio greater than 100%. Gerber (1980) invented a saturated hygrometer to measure the supersaturation ratio in the fog based on the scattering properties of droplets on a membrane. He used a saturated hygrometer to perform a number of observations in the fog and found that the supersaturation ratio in the radiation fog was up to 0.5% (Gerber, 1981), which was much greater than the estimated value

in the radiation fog in the literature (Bott et al., 1990; Roach, 1976). This method was an indirect measurement with relatively large errors. Saturation ratio can also be measured through a combination measurement of water vapor partial pressure and temperature. Water vapor concentration can be measured by a Licor H_2O analyzer (LI-COR, Inc.; Korolev & Isaac, 2006) based on the absorption of infrared radiation by moist air, whose declared accuracy for measurements of absolute humidity is 1% and the uncertainty is also too large.

On the other hand, the measurement of supersaturation also requires high time resolution. In the ambient environment, the temperature and water vapor density at a certain point show time-dependent pulsation that also performed on real-time supersaturation ratio. Therefore, it is a big challenge to perform measurements with such high frequency that can reach 10 Hz to record the real fluctuations of the ambient supersaturation.

In previous studies, water vapor supersaturation is often involved in the interaction between aerosols and clouds or fogs (Gerber, 1991; Herich et al., 2009; Mazoyer et al., 2016; Su et al., 2017). Water droplets form by condensation of water vapor on the aerosol particles. The Köhler theory forms the basis of our understanding of cloud droplet formation (Kohler, 1936). Motivated by this theory, CCN calibrations are performed where particles of known chemical composition are exposed to an unknown supersaturation (Nan et al., 2014). According to the activation characteristics these particles ultimately show, the column supersaturation can be determined. Similar to this idea, the environment can be compared to a big open column, in which ambient particles are exposed to a supersaturation. If we have known aerosol particles' properties and the activation characteristics the particles appear, the effective supersaturation during this process may be deduced through the Köhler theory. However, the activation process of ambient particles is much more complex when compared to the experimental setup in the laboratory in two aspects: ambient particles are complex mixtures composed of different components and will consequently show more complicated activation properties (Ren et al., 2018; Zhang et al., 2017); the supersaturation ratio in the environment is much more unstable, as being influenced by various surrounding factors. In addition, under saturation condition, most aerosol particles can take up water and grow to a much larger size only through hygroscopic growth and some of them may even reach the level of micrometer. Because of the similarities these hydrated particles share with activated droplets, sometimes it is difficult to distinguish between them in the measurement. Especially for heavy-polluted areas such as the North China Plain where large number concentration of aerosol particles can be found, hydrated particles can contribute a lot to the formation of visibility degradation events like fogs or haze. To the best of our knowledge, there has not been any study trying to combine the hygroscopic growth and activation process together to obtain the supersaturation ratio.

In this work, a novel method is proposed to estimate the water vapor supersaturation during the ambient activation process based on the data set of aerosol particle number size distribution (PNSD), aerosol hygroscopic properties, and droplet measurements. The κ-Köhler theory, which have a single parameter κ, is employed to describe the aerosol hygroscopic growth and aerosol activation process (Petters & Kreidenweis, 2007). Based on the κ-Köhler theory, the droplet data can be determined when given the data of κ, PNSD, and supersaturation. The water vapor supersaturation can be constrained by comparing the predicted droplet data with the measured one.

While it is difficult to observe the microphysical properties of the cloud, fog appears in ground layer, which can be considered as a type of low-lying cloud. It provides us a convenient platform to study the supersaturation in the aerosol activation process in the natural environment. Therefore, we will apply our method to a fog episode to evaluate its applicability. In this paper, section 2 describes instrumentation used for the measurements and data set. Section 3 describes the method in detail including an overview of κ-Köhler theory and derivation algorithm of supersaturation ratio. Section 3.1 illustrates the application of the proposed method to a fog episode and discussion of results, and section 4 is the conclusions we have obtained.

2. Experiment and Instrumentation

2.1. Experiment

This study is part of the project Haze in China (HaChi), which was conducted by the collaboration of Peking University, China, and Leibniz Institute for Tropospheric Research, Germany. In addition to the intensive field campaign in July–August 2009, a fog and haze experiment of the HaChi project was carried out at Wuqing

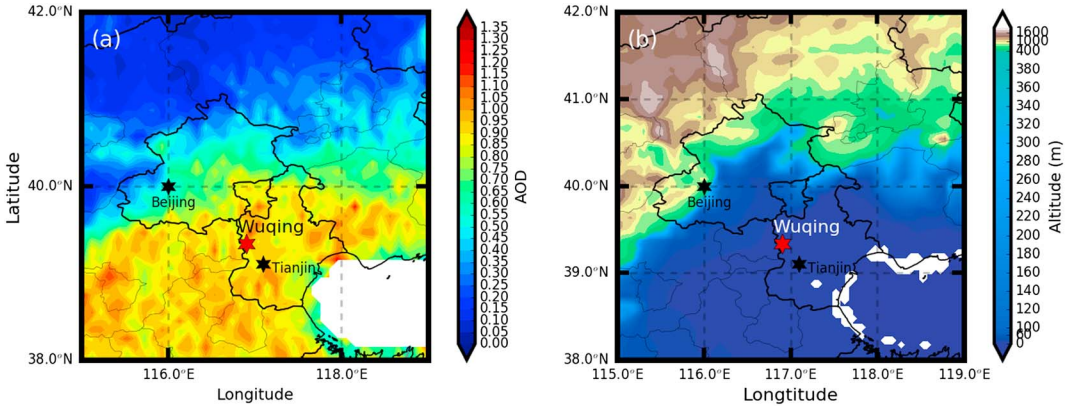

Figure 1. The maps show the site location (red star), major cities in the vicinity (black stars). (a) The 3-year (13–16) average AOD (aerosol optical depth) derived from the Moderate Resolution Imaging Spectroradiometer (MODIS). (b) The altitude distribution.

from the end of October 2009 to late January 2010. The aim of this experiment was to obtain more insight into the physical characteristics of fog process. The measurement site, Wuqing meteorological station (39°23′N, 117°01′E, 6 m a.s.l.), is a rural area between Beijing and Tianjin, the two heavily populated megacity centers, as shown in Figure 1. It is nearly 80 km to the southeast of the Beijing and 30 km to the northwest of the Tianjin. Most of the neighboring industrial sources are clustered to the east of the site. To the west of and south of Wuqing, the landscape is generally agricultural oriented in land use and land cover. Traffic flow near the site is on a very low level, and there are no large emission sources in the surrounding areas nearby. Overall, Wuqing lies inside the polluted region and is highly representative of the overall pollution level of the polluted North China Plain (NCP) region and a favorable spot for observing transport of air pollutants. More detailed site descriptions can be found in Ran et al. (2011) and Liu et al. (2011). During the fog experiment, ground-level measurements of aerosol size distribution, droplet size distribution, visibility, and meteorological parameters were performed.

2.2. Instruments

In our study, three fog cases from 6 to 8 November were analyzed here. The data used in this work include temperature, wind speed and directions, visibility, the dry particle number size distributions (PNSDs), hygroscopic properties of aerosols, and droplet size distribution in the fog observations.

Meteorological variables were obtained by an Automatic Weather Station installed at the Wuqing Meteorological Station. Temperature was collected at 1.5-m height using the Vaisala HUMICAP humidity and temperature probe (HMP45) with an accuracy of ±0.2 °C at 20 °C. Wind parameters were observed at 10-m height. The wind speed was measured using a EL15-1A cup wind speed sensor with an accuracy of 0.3 m/s (≤10 m/s), while the wind direction was measured using a EL15-2D wind direction sensor with an accuracy of ±3°. They all had a time resolution of 1 min. The visibility was measured using a forward scattering measuring visibility meter (Model FD12, Vaisala Corporation, Finland) with a temporal resolution of 15 s.

Online PNSDs data were obtained using a scanning mobility particle sizer (SMPS) which consists of a differential mobility analyzer (TSI 3071) to select particles with size of 10 to 700 nm and a condensation particle counter (TSI CPC 3022) to count particle numbers in a narrow size range. The sampled air mass first entered through a dryer which reduces the relative humidity (RH) to less than 30% in order to get the PNSDs in dry condition. The temporal resolution of the PNSD data was 5 min. More details can be found in Ma et al. (2011).

The droplet size distribution at ambient humidity was measured using the Fog Monitor (Model FM-100) from Droplet Measurement Technologies (DMT). Its measured particle size range is 2–50 μm with a temporal resolution of 1 min. In order to be consistent with the resolution of SMPS measurements, the FM-100 data used here were averaged over 5 min. The aerosol hygroscopicity is measured using the high humidity tandem differential mobility analyzer (HHTDMA) which measures the aerosol growth factor (GF) as a function of RH at different diameters. The aerosol hygroscopicity parameter κ can be directly derived from measurements of the HHTDMA (Liu et al., 2011). The size-resolved κ within whole size range can then be obtained based on

the four-mode fitting method (Chen et al., 2012) from HHTDMA and PNSD data. However, in this field observation, the real-time measurement of aerosol size-resolved hygroscopicity is absent. Since this fog episode occurred in a relative calm weather conditions, and as a result, the aerosol particles had gone through long-time aging processes and had a relative stable distribution of chemical compositions. The averaged κ may to some extent represent the average chemical compositions in this area, so we adopted an average size-resolved κ distribution representative of this place.

3. Method

3.1. κ-Köhler Theory

The relationship between the diameter D of a single (spherical) particle and the equilibrium ambient water vapor saturation ratio can be well represented by Köhler theory (Kohler, 1936)

$$S(D) = a_w \exp\left(\frac{4\sigma_{s/a} M_w}{RT\rho_w D}\right) \tag{1}$$

where S (D) is the saturation ratio over the hydrated particulate solution surface, a_w is the water activity of the condensed (aqueous) phase present in the droplet, $\sigma_{s/a}$ is the surface tension coefficient, M_w is the mole mass of water, R is the universal gas constant, T is the temperature, and ρ_w is the density of water. The equilibrium calculations carried out for typical aqueous solutions using equation (1) yield the well-known Köhler curve, and it can predict the minimum supersaturation (Sc) required for a particle to activate into a cloud droplet. Recently, a single-parameter representation of the Köhler equation has been proposed (Petters & Kreidenweis, 2007) where a widely used hygroscopicity parameter κ is introduced to analyze the hygroscopic growth of particles in the subsaturated and supersaturated regime. Based on the Köhler equation, the physical quantities about aerosol hygroscopicity are simplified to a single parameter κ to obtain a new equation, named *κ-Köhler theory*. According to this theory, S (D) can be calculated from

$$S(D) = \frac{D^3 - D_d^3}{D^3 - D_d^3(1-\kappa)} \exp\left(\frac{4\sigma_{s/a} M_w}{RT\rho_w D}\right) \tag{2}$$

where D_d is the diameter of the dry particle. When $S < 1$, it is equivalent to RH/100 and when $S > 1$, supersaturation is defined as $(S - 1)$.

From equation (2), there exists a critical size at which the Raoult effect just balances the Kelvin effect. Below that size, we call the water uptake of particle as *hygroscopic growth*; above that size, we call the particle *activated*. Here we assume that when a dry particle is exposed to a RH, it follows an equilibrium path along the S (D) trajectory as it takes up water before activation. So the wet equilibrium diameter can be calculated using the *κ-Köhler equation*. By comparing the Sc with ambient supersaturation, the activation condition can also be determined.

However, the application of equation (2) requires assumptions regarding the surface tension and the temperature; thus, it is recommended that equation (2), and related equations, be applied for T = 298.15 K and for $\sigma_{s/a}$ equal to that of pure water at that temperature. Large errors may occur with the presence of surfactant organic species. The variability in solubility and volatility of aerosol constituents can also influence the accuracy of this parameterization scheme. For example, some species may be more readily dissolved under a higher RH that will thus appear more hygroscopic correspondingly.

3.2. An Analysis on Activated and Unactivated Droplets

Droplets are typically composed of two kinds of particles: microsize hydrated (unactivated) particles which grow from aerosol particles by hygroscopic growth and maintain an equilibrium size with ambient humid air and activated particles which will grow spontaneously if the ambient supersaturation remains at or above the respective equilibrium value. However, sometimes it can be difficult to distinguish unactivated droplets from activated droplets in real fog or cloud process because they share similar optical properties and droplet sizes (Frank et al., 1998). In previous studies, there are different methods to separate these two kinds of fog droplets and one of them is to set a fixed value as a rough boundary between them; for example Elias et al. (2009) used 2 μm as the dividing size of accumulation mode aerosols and fog droplets. Droplets of diameter larger than the fixed value will be considered activated while the others be considered haze particles.

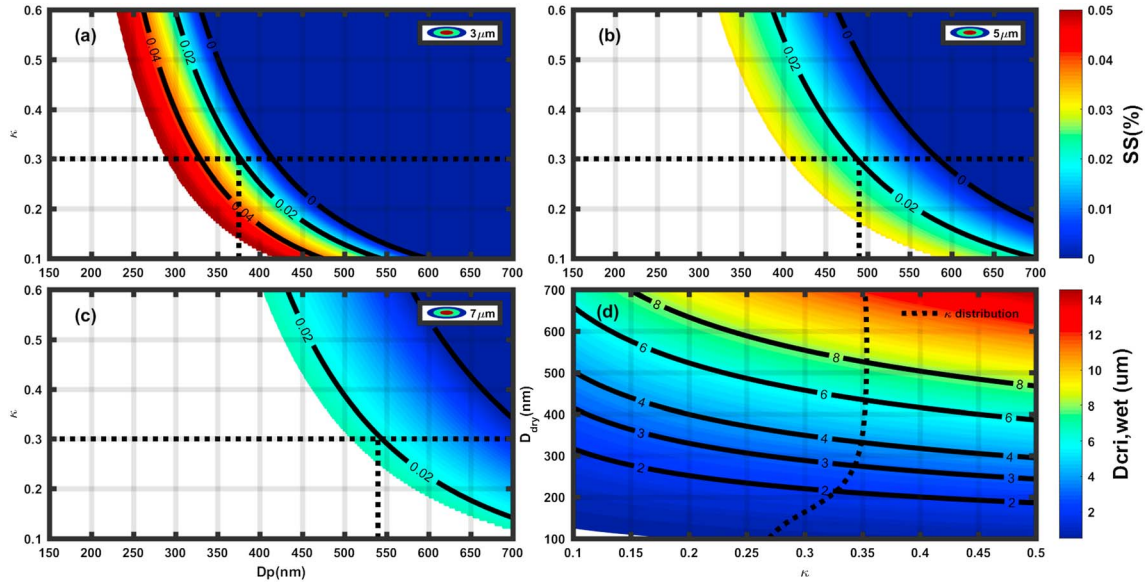

Figure 2. (a–c) The dry diameter of a particle that can grow to the corresponding droplet size (3, 5, and 7 μm) through hygroscopic growth without activation. The blank areas on the left of the colored areas are regions where the particle is activated. The color represents the supersaturation, and the value it stands for can be determined through the color bar on the right. The numbers on the contour line also indicate the supersaturation value. (d) The wet critical diameter calculated using κ-Köhler theory from dry diameter and κ. The black dotted line represents the average size-resolved κ distribution in this area.

However, using κ-Köhler equation, we have found that an aerosol particle can grow up to the cloud drop size through hygroscopic growth without being activated. Figures 2a–2c show the particle's hygroscopic growth with a hygroscopic parameter κ of 0.3 at a supersaturation of 0.02%. A particle of 370-nm size can grow to a 3-μm droplet, a particle of about 500-nm diameter can grow to a 5-μm droplet, and a particle of about 550-nm diameter can grow to a 7-μm droplet. Therefore, at a relatively low supersaturation, particles, especially large particles with high hygroscopicity, can grow without activation to the droplet sizes that are conventionally considered to be representative of activated droplets. Contrary to this, at a relatively high supersaturation, few particles can grow to large droplets only through hygroscopic growth because most of them will directly activate into cloud droplets. The blank area on the left of colored area in Figures 2a–2c is the region where particles have been activated. It can be seen that at a supersaturation of about 0.05%, only a few particles can grow to 3 μm through hygroscopic growth, and nearly no particles can grow to a larger size of about 5 or 7 μm without activation.

For the observation site, the number of droplets grown from hygroscopic growth cannot be neglected. Jointly controlled by microphysical process and meteorological factors (Shen et al., 2015; Su et al., 2018), the aerosol number concentration can be quite large. With the assumption that the ambient RH in the fog is approximately 100%, we obtained the wet PNSD under 100% RH condition from dry PNSD (RH $<$ 100%) measured by the SMPS and size-resolved κ using κ-Köhler theory (Hammer et al., 2014). The dry PNSD and κ were measured in the observation site that can be considered representative of heavily polluted locations in the North China Plain. Figure 3a shows the occurrence of all the dry PNSD during the fog episode. Corresponding recalculated wet PNSD is shown in Figure 3b. Under this condition, all the wet particles were grown from hygroscopic growth. It can be seen that the number concentration of hygroscopic droplets larger than 2 μm can reach the magnitude of hundreds per cubic centimeter and account for about 1% of the total particles. When the number concentration of particles increases (heavily polluted), this part of droplets will also increase which will make a significant contribution to the light extinction and visibility degradation without activation.

Apart from unactivated hydrated particles, we also calculated the wet critical diameter for activated particles (Figure 2d). These particles have dry diameters ranging from 100 to 700 nm and hygroscopic parameter κ ranging from 0.1 to 0.5. The dotted line in Figure 2d represents the average size-dependent κ in the observation site. From Figure 2d, we can see that for particles larger than about 330 nm, the wet critical diameter is larger than 4 μm which is meant to be the minimum diameter (D_{min}) for activated droplets.

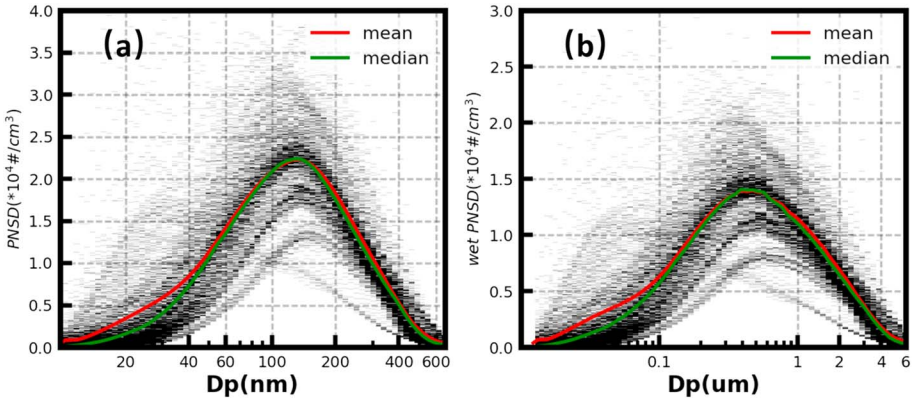

Figure 3. (a) All particle number size distribution (PNSD) measured at a relative humidity of less than 30% during the fog episode. (b) The corresponding wet PNSD at a relative humidity of 100% calculated with κ-Köhler theory. The gray color represents the frequency of PNSD, and darker points correspond to a higher frequency. The red and green lines represent the mean and median PNSD, respectively.

In this study, instead of treating droplets as being activated, we reserve the possibility of droplets being grown by hygroscopic growth or activation process. The activated and unactivated droplets can share the same size, but we avoid the need to distinguish between them in the beginning of calculation. When we apply our method to a fog episode, $D_{\min}$ of 4 μm will be presumed. Detected fog droplets larger than 4 μm will be composed of all the activated droplets and part of unactivated haze particles.

3.3. Derivation Algorithm for Supersaturation

The iterative process used to derive the effective ambient supersaturation is illustrated in Figure 4. The ultimate purpose of this iterative algorithm is to find a supersaturation under which the predicted droplet number concentration ($N_{d,\text{pred}}$) can match the observed one ($N_{d,\text{obs}}$) best. So determination of $N_{d,\text{pred}}$ from dry aerosol size distributions and aerosol hygroscopicity properties at a given supersaturation is one of the most important processes in the analysis. It is to be noted that when comparing $N_{d,\text{pred}}$ with $N_{d,\text{obs}}$, it is necessary to select a threshold diameter, which means that droplets number concentration above this size are compared. Here in our method, we will choose the $D_{\min}$ of 4 μm as the threshold for two reasons. One is for computational convenience because the second size bin of fog monitor starts from 4 μm, and 3 μm of threshold will involve interpolation. On the other hand, from Figure 3 we can see that when the threshold is relatively low like 2 or 3 μm, large number of aerosol particles will theoretically grow to be larger than the threshold, and in some cases, the calculated number concentrations above threshold may even much larger than the measured total number concentrations. But in the ambient environment, the number of droplets cannot reach that high because of water vapor competition especially under heavily polluted conditions. So a relatively large threshold is necessary to avoid this contradiction. But a large threshold will also lead to an underestimation of calculated supersaturation because it may exclude some activated droplets. Overall, a threshold of 4 μm seems the best choice that can balance these two considerations. Then the predicted droplet number concentration is computed by

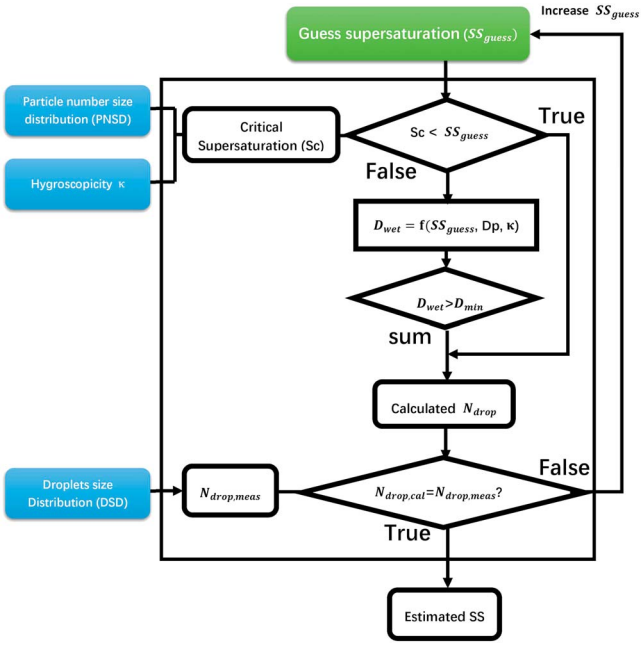

Figure 4. Schematic representation of the iterative algorithm for calculating supersaturation ratio during the ambient activation process: an inverse application of κ-Köhler theory.

$$N_{d,\text{pred}}(>D_{\min}) = N_{\text{activated}} + N_{\text{unactivated}}\left(D_{\text{wet,equilibrium}} > D_{\min}\right) \quad (3)$$

A particle can either activate or just grow to an equilibrium size with the presumed supersaturation. We suppose that all particles with a critical supersaturation (S_{cri}) smaller than the ambient supersaturation are

activated. From equation (2), if size-resolved hygroscopic parameter κ is available, we can determine whether the particles on known size bins can be activated with an assumed supersaturation. If particles are activated, then the total number concentration of this size bin can be added to the predicted total droplet number concentration. Else, but if the hygroscopic equilibrium droplet size calculated using equation (2) is larger than D_{min}, these aerosol particles can also be added to the droplet population $N_{d,pred}$. Above all, the predicted droplet number concentration can be determined as a function of the water vapor supersaturation.

The observed droplet number concentration is computed as

$$N_{d,obs} = \Sigma_{D_{min}}^{D_{max}} \Delta n(D), \tag{4}$$

where Δn (D) represents the droplet size distribution measured per size bin around the diameter D, per air volume unit. If the $N_{d,pred}$ is closest to the $N_{d,obs}$ at a presumed supersaturation, we can consider this value as the effective supersaturation. In the calculation, there are several methods to reduce the computation amount. One of them is the use of interpolation. We do not need to calculate every $N_{d,pred}$ corresponding to a finite step increase of the supersaturation. A suitable interpolation will greatly reduce the computation amount while maintaining the accuracy. Another method is the bisection search that needs the bounds of the supersaturation at first. This method is built on the basis that the droplet number concentration increases monotonically with the supersaturation.

3.4. Aerosol Hygroscopicity κ

In the retrieval of the effective supersaturation, the aerosol hygroscopicity and mixing state play a crucial role in the hygroscopic growth and activation process of ambient aerosol particles, especially at low supersaturations (Twohy & Anderson, 2008). Aerosol hygroscopicity can be measured with many methods (Jaatinen et al., 2014). Under supersaturated conditions (RH $>$ 100%), size-resolved activation ratios derived through CCN measurements contain information regarding the effects of size-resolved chemical compositions and mixing states on aerosol activation properties (Deng et al., 2013). The inferred critical diameter (*Dc*; corresponding to an activation ratio of 0.5) combined with the column supersaturation can give an estimate of the κ using κ-Köhler theory. Under subsaturated conditions (RH $<$ 100%), the Hygroscopic Tandem Differential Mobility Analyzer (HTDMA) instrument can be applied to measure the hygroscopic GF at different RHs for particles of different diameters. The hygroscopic growth behaviors at different RHs can then be fitted to the κ-Köhler equation, and the measured GF probability distribution can be converted to a κ distribution of corresponding diameter (Liu et al., 2011). Additionally, analysis on measured particle chemical composition can also help to derive a hygroscopicity parameter κ (Liu et al., 2014). From these methods, various types of κ can be obtained, for example, averaged κ over all particles, size-resolved κ indicating size-dependent hygroscopic characteristics, and κ probability distribution which can provide further insights into aerosol mixing state.

The computational process and results may vary a little among different types of κ. For example, if κ probability distribution function is available, particles in one size range cannot be treated as exhibiting the same hygroscopic properties. Instead, we can obtain the GF distribution and subsequently the fraction (F (D_d, SS)) of particles that can grow to be larger than D_{min}. Then the total predicted droplet number concentration ($>D_{min}$) can be calculated as

$$N_{d,pred} = \Sigma_{D_d} \left(\frac{dN_{CN}(D_d)}{d \log D_d} \right) \cdot F(D_d, SS) \tag{5}$$

If an average κ over all sizes is provided, then the iterative algorithms can be simplified a lot. Since all particles have a same κ, then the diameter will become the deciding factor to determine whether a dry particle can make a contribution to the $N_{d,pred}$. On the condition that larger particles more readily grow to larger droplets, the critical diameter can be deduced from the measured droplet number concentration and PNSD when integrating the PNSD from each size diameter bin to the largest measured particle diameter to match the total droplet number concentration. Combined with the κ, supersaturation can be obtained.

In addition to the κ forms, there can also be an inconsistency between κ values estimated from different methods especially for some organic species (Petters et al., 2009; Prenni et al., 2007) because there are

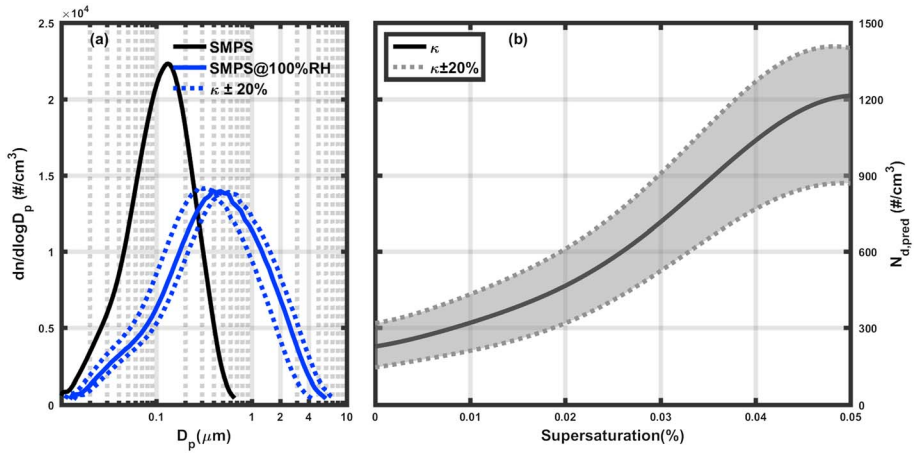

Figure 5. (a) The solid black line represents the average dry particle number size distribution during the fog episode, and the solid blue line represents the corresponding wet PNSD at a relative humidity of 100% calculated with κ-Köhler theory. The dotted blue line represents the wet PNSD when the κ is changed by 20%. (b) The $N_{d,\mathrm{pred}}$ calculated given a specific supersaturation. The dotted gray line represents the $N_{d,\mathrm{pred}}$ when the κ is changed by 20%. PNSD = particle number size distribution; SMPS = scanning mobility particle sizer.

several important factors that can influence the hygroscopic behavior of aerosols, for example, the solubility, surface tension, and deliquescent point, which may all have something to do with RH. The RH range in the HTDMA may be insufficient to deliquesce all the constituents in the particles, or some organic compound may be more readily dissolved in CCN experiments, which will make a *hygroscopicity gap* between CCN and HTDMA measured κ. We have evaluated the sensitivity of $N_{d,\mathrm{pred}}$ to κ, and the results are shown in Figure 5. The dry particle size distribution was obtained by averaging the SMPS data during the fog episode. The dotted lines in Figures 7a and 7b represent the results when changing the hygroscopicity by 20%. From Figure 5b, it can be seen that $N_{d,\mathrm{pred}}$ varies greatly with κ, and the variation of $N_{d,\mathrm{pred}}$ can be up to 40%. So in our study, κ measured under high RH is preferred since it can better represent the particles' hygroscopic behaviors around 100% RH.

Regardless of the computational efficiency and measurement difficulty, the more detailed the information about the hygroscopic properties is, the more accurate the results are. Previous studies showed that aerosol hygroscopicity is highly size dependent, and size-dependent information on composition is needed to predict CCN concentrations relevant to cloud droplet formation (Jaatinen et al., 2014). In our calculation, we will use a size-resolved κ deduced from HHTDMA measured GF (under 90%, 95%, and 98.5% RH) to represent aerosol particles' hygroscopicity. For regions far from strong aerosol primary emissions, the influence of mixing state on aerosol cloud activity is small and the assumption of internal mixing state in a particular size is sufficient for the calculation of $N_{d,\mathrm{pred}}$ (Dusek et al., 2006; Ervens et al., 2010). But this selection of κ might not be applicable for regions or air masses greatly affected by strong primary aerosol emissions.

4. Application in a Fog Episode

4.1. Overview of the Fog Episode

We applied this newly proposed method to a strong radiation fog observed by HaChi from 6 to 8 November 2009 to estimate the supersaturation ratio in the process. During the fog episode, the fog droplet number concentration reached 800 cm^{-3}, the liquid water content reached 0.5 g/cm^{-3} and visibility dropped down to 50 m. The time series of temperature, wind speeds and directions, visibility, droplet size distribution, and dry aerosol size distribution are displayed in Figure 6. Basic physical parameters of the fog cases in the North China Plain are also measured simultaneously.

From Figure 6, we can see that this fog episode contained three cases. The first case started midnight from 3:00 a.m. to 11:00 a.m. on 6 November; the second case took place from 21:00 on 6 to 12:00 on 7 and the third case lasted from 17:00 on 7 to 5:00 a.m. on 8. With temperatures above 0 °C, these fogs can all be considered as liquid fogs in this study. We can also see an obvious falling air temperature upon the fog formation. During

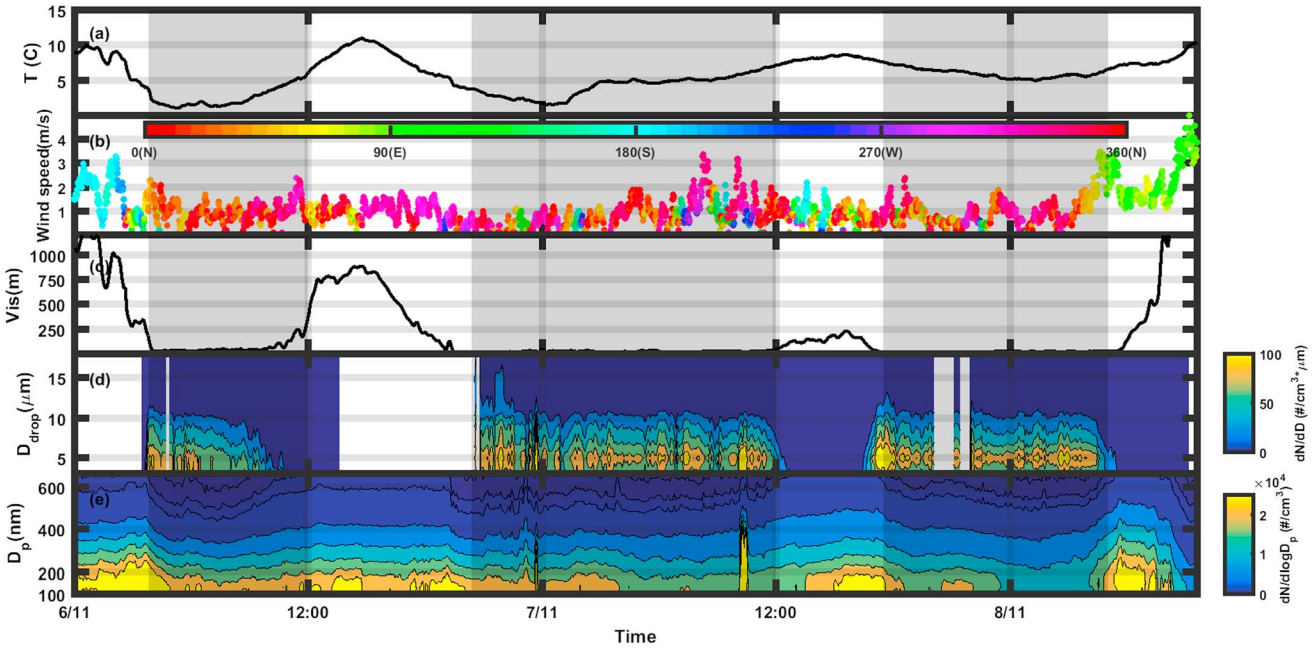

Figure 6. The time series of (a) temperature, (b) wind speed and direction, (c) visibility, (d) droplet size distribution, and (e) dry particle number size distribution during the fog episode. The gray area represents the three fog cases in the episode. Droplet-related parameters have time resolution of 1 min, while the aerosol-related parameter has time resolution of 5 min.

fog pertain, the wind speeds are mostly no larger than 2 m/s and the average wind speed was 0.88 m/s, which implied a calm and stable weather condition. Droplet size distributions of these fog cases have only one mode, with a modal radius of about 2–3 μm. The shape of the spectra also does not change much throughout the development of the fog. It can also be seen that the aerosol count is much smaller during fog pertain because of wet deposition; for example, particles were collected by droplets as a result of in-cloud scavenging due to impaction or diffusion. The averaged properties and their associated standard deviations when N_{drop} is larger than 100 cm^{-3} for each case are summarized in Table 1. It can be seen that N_{drop} and N_{aer} are quite large. N_{drop} is on the order of 500–600 cm^{-3}, N_{aer} is on the order of 10^4, and liquid water content (LWC) is about 0.2–0.3 g/cm^3 on average. They can all be classified as dense fogs.

In the in situ observations, the SMPS we used to measure the particle size distributions online has a measurement range of 10–700 nm, which means that ultrafine particles of diameter less than 10 nm and coarse particles of diameter more than 700 nm were not included in the size distribution. For particles less than 10 nm, normally they would not grow to a droplet larger than D_{min} in any case. Even ammonium sulfate (κ = 0.61) particles can only take up water to the wet equilibrium diameter of less than 20 nm under the supersaturation value of 1%. Therefore, the absence of this part of particles has no effect on the $N_{d,pred}$. But for coarse particles greater than 700 nm, they could easily grow to contribute to $N_{d,pred}$. From Figure 2 we can see that at a supersaturation of 0.02%, a 700-nm particle with κ of 0.1 can grow to 5 μm; a more hygroscopic particle will grow to 5 μm even under subsaturation through hygroscopic growth. Take ammonium sulfate particles for example, the supersaturation ratio of 0.01% can completely activate particles larger than 600 nm. Even for completely nonhygroscopic particles (κ = 0), the supersaturation ratio of 0.3% is sufficient to allow particles larger than 700 nm to be activated. Therefore, this missing part could make a difference. In the HaChi observation, we used a Twin Differential Mobility Particle Sizer (TDMPS, IfT, Leipzig, Germany) and an Aerodynamic Particle Sizer (APS Model 3320, TSI, Inc.) to analyze the aerosol size distribution in winter and summer, respectively. The combined measurement of TDMPS and APS ranges from 3 nm to 10 μm, which can be considered to cover all size ranges of aerosol particles. The results showed that the average concentration of particles larger than 700 nm is 13 and 20 cm^{-3} in winter and summer, respectively. So the number

Table 1
A Summary of the Averages and the Standard Deviations of N_{drop}, Droplet Mean Diameters, LWC, and N_{aer} in the Three Fog Cases

Variables	Case 1	Case 2	Case 3
N_{drop}(cm^{-3})	503 ± 166	609 ± 174	577 ± 168
Mean diameter (μm)	6.3 ± 0.6	7.0 ± 1.6	7.0 ± 1.8
LWC (g/m^3)	0.21 ± 0.09	0.31 ± 0.15	0.28 ± 0.12
N_{aer}(*10^3 cm^{-3})	18.8 ± 2.5	15.5 ± 3.7	14.1 ± 5.2

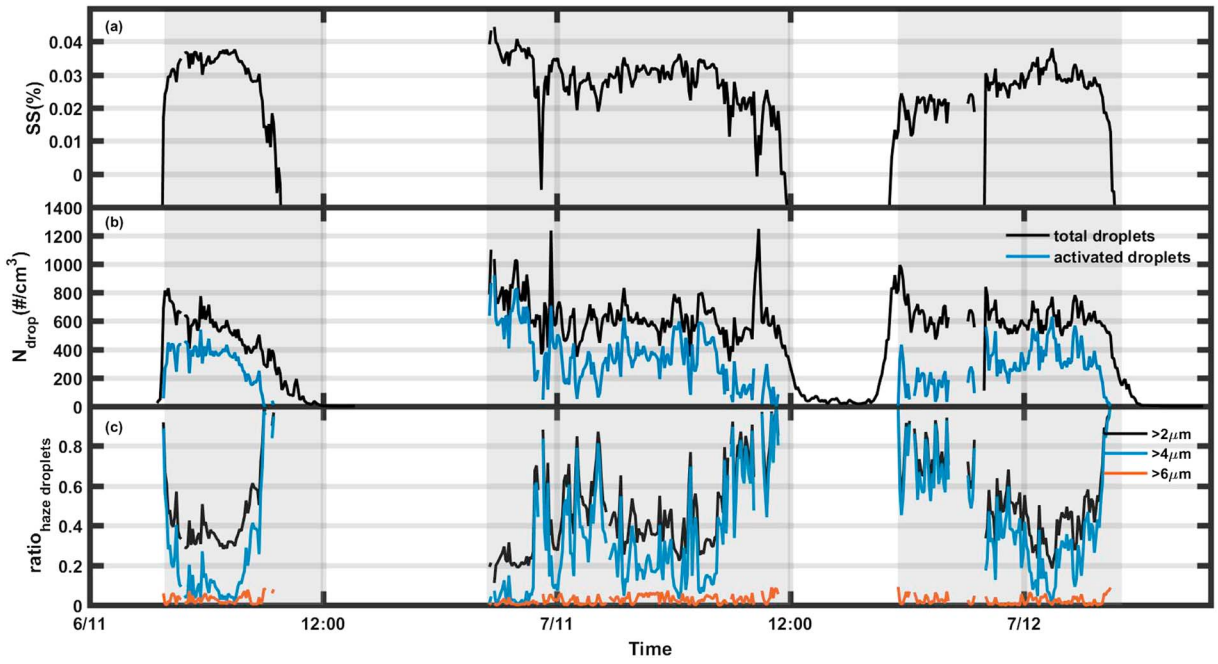

Figure 7. (a) The time series of calculated supersaturations. (b) The time series of number concentrations of total droplets (>2 μm) and activated droplets. (c) The ratio of unactivated haze droplets to total droplets above 2, 4, and 6 μm, respectively.

concentration of this missing distribution of particles is negligible relative to the concentration of droplets. Therefore, we ignore the effect of particles above 700 nm on the calculation of $N_{d,\mathrm{pred}}$.

4.2. Results and Discussions

Based on the iterative algorithm proposed above, supersaturation values as well as calculated activated droplet number concentrations are derived from the aerosol and droplet measurements. The time series of droplet (measured and calculated activated) number concentrations and supersaturation values are shown in Figure 7.

During the three fog cases, the calculated supersaturations vary from 0.01% to 0.05%. In the dissipation process, the supersaturations may drop down to 0 or a minus value. The maximum supersaturation is quite low no larger than 0.05%. In previous studies, Gerber (1991) found in a radiation fog that nongradient turbulent mixing can cause an average shape of supersaturated eddies with a median peak supersaturation of 0.049%. Mazoyer et al. (2016) also tried to obtain the supersaturation through aerosol and droplet measurements and derived a critical supersaturation with a median of 0.043% during the winters of 2010–2013 at the SIRTA observatory in the suburb of Paris. The results of our method do not deviate much from these measurements or calculations, and the relative low values can be explained by the heavy pollution in the NCP. The correlation coefficient between the supersaturation and temperature is −0.66, and the correlation coefficient between supersaturation and the number concentration of aerosol particles larger than 300 nm is −0.58, both showing a weak negative correlation. These two values to some extent explain that the supersaturation ratio in the environment is negatively affected by the temperature and CCN-active aerosol particles, as the warming raises the equilibrium vapor pressure of water and the depletion of excess vapor is enhanced by more CCN-active aerosol particles.

The supersaturation ratio calculated with this method is in fact an effective supersaturation. The *effective* here means that the calculated supersaturation can produce the same droplet number concentration with the measurement. In the calculation, it is nearly impossible to accurately describe and track the particles' activation process as well as its water uptake growth, because the time resolution of droplets and aerosol measurement is 1 and 5 min, respectively, so the realistic supersaturation pulsation cannot be depicted. On the other hand, aerosol particles are in a continuous mutual interaction with ambient supersaturation. Therefore, similar to the principle of the supersaturation ratio calibration in the DMT CCN counter, the specific process of

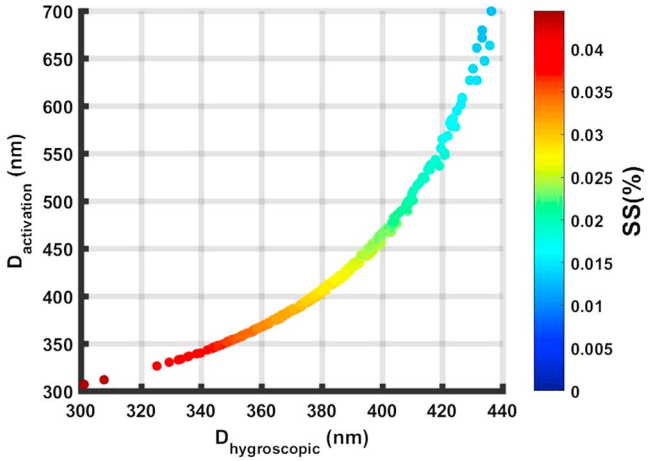

Figure 8. Comparisons between the minimum diameter of particles that can grow to 4 μm and the critical activation diameter; the colors of the dots present their corresponding supersaturations.

particle water uptake growth as well as activation and the fluctuation of the supersaturation ratio in the ambient activation process are neglected in the calculation method. In other words, only the quasi stable states before and after the activation process are used and the supersaturation ratio is estimated according to the activation conditions the aerosol particles ultimately show. Thus, the obtained supersaturation ratio is an effective value and is not exactly equal to the instantaneous supersaturation ratio in the environment. That is also the reason that the calculated supersaturation state from Figure 7a seems to pertain for several hours without any moment of subsaturation, which seems hard to envision in the ambient fog episode. In the temporal resolution time range, supersaturation fluctuations due to turbulence could possibly produce a droplet distribution that pertains for a while to make a supersaturation calculation result. These spike supersaturations may be smoothed out by current measurement that is based on spatial-temporal averaging.

The ratio of haze droplets to total droplets above a size threshold, like 2, 4, and 6 μm, is also illustrated in Figure 7c. In the figure, the unactivated micron-sized haze particles constitute quite a part of the total detected fog droplet number concentrations but the percentage they account for is decreasing with droplet size. For droplets larger than 2 μm, the average ratio of unactivated haze particles to droplets is about 0.5; for droplets larger than 4 μm, the average ratio is about 0.3; and for 6 μm, this value is quite low about 0.03. The decreasing trend of haze particles' ratio may be explained that the size that aerosol particles can grow to through hygroscopic growth is not large, and in this case, the upper limit is about 6 μm.

Compared to conventional CCN observations under controlled supersaturation conditions, the calculated supersaturation ratios are mostly lower than the minimum supersaturation ratio (0.07%) set by the CCN counter (DMT) that has been widely used. The colored dots in Figure 8 represent the minimum diameter for particles to be activated (y label) or grow up to 4 μm through hygroscopic growth (x label) under different supersaturation condition. These supersaturations all occurred throughout the fog episode. It can be seen that almost all the particles that can be activated were larger than 330 nm, which is a verification of the selection of D_{min} discussed in section 3.2. For conventional CCN observation, they were operated at a supersaturation of more than 0.07%, which reflect the activation properties of particles smaller than 300 nm (e.g., Deng et al., 2011). Therefore, for ambient activation processes with equivalent supersaturation ratio well below 0.07%, the conventional observations of aerosol size-resolved activation ratios need to be improved with a much lower supersaturation ratio.

4.3. Sensitivity Analysis

In the activation process, droplets number concentration could change because of droplet coalescence, sedimentation, and breakup, and the calculated supersaturation will also change correspondingly. In previous studies (Lamb & Verlinde, 2011), the maximum values of collision efficiency are low for small collector drops and 40 μm is considered to be a threshold diameter. In our observation, the droplets larger than 40 μm constituted no more than 1% of the total droplets; thus, coalescence will not have an appreciable effect on the fog droplet size spectra. Twomey (1966) has also shown that coalescence does not greatly alter an initial droplet spectrum (having a mean diameter as large as 30 μm) even after 30–60 min. Breakup effect can also be neglected because drops may be as large as 4.5 mm in equivalent radius before breaking up in quiet air (Pruppacher & Klett, 2004). However, errors may occur in the in situ measurement. In the FM-100, due to the uncertainty in the correction between Mie scattering and droplet size, as well as the particle losses during sampling, the error of the measured total number concentration is estimated within an uncertainty of 10% according to Spiegel et al. (2012). Here we increased and decreased the observed droplet number concentration by 10% to reveal the corresponding variability of derived supersaturations. In Figure 9a, it can be seen that 10% change of droplet number concentration will cause the calculated supersaturations to shift by a value of 0.005%.

In addition to measurement errors in the droplet number concentrations, the hygroscopic properties have also contributed significantly to the deviation of supersaturation. Because of the absence of simultaneous

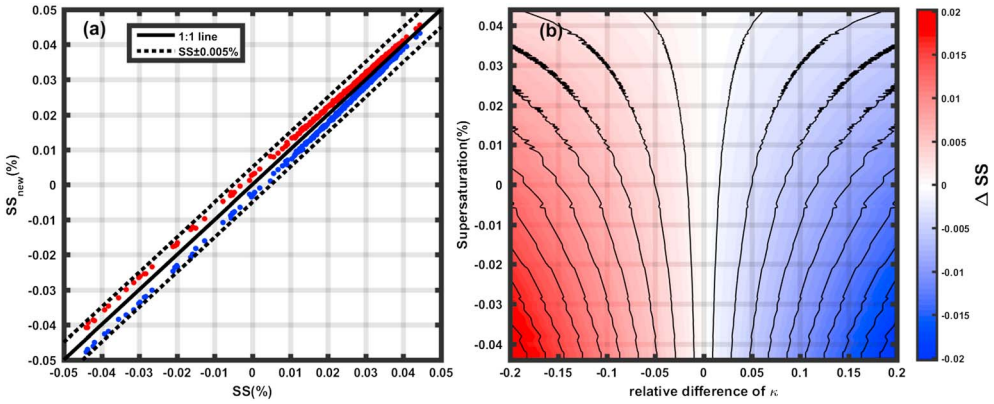

Figure 9. (a) The *x* axis represents the original supersaturations, and the *y* axis represents the supersaturations obtained after increasing (red dots) or decreasing (blue dots) the observed droplet number concentrations by 10%. The black line is the 1:1 line, and the two dotted lines shifted up and down by a distance of 0.005%. (b) Contour colors represent the difference of calculated supersaturations when changing the hygroscopic parameter κ by a factor from −20% to 20%.

real-time aerosol hygroscopicity measurement, the aerosol's instantaneous hygroscopicity would possibly deviate from the average one. The complex mixing state of ambient aerosol particles was also not included in consideration. Moreover, organic species like some surfactants may evaporate during the drying process before the measurement, which will cause the underestimation of particles' apparent κ. While everything else is equal, the presence of surfactants can enhance particles' hygroscopicity and thus produce a lower supersaturation. So a sensitivity analysis from hygroscopic parameter κ by a factor from −20% to 20% was performed. The difference in calculated water vapor supersaturation resulting from the deviation of κ is shown in Figure 9b. Supersaturation estimates are on the high side when κ is underestimated, whereas overestimation of κ will result in a lower value of calculated supersaturation. Meanwhile, according to the gradient of the color, the lower-derived supersaturation is more sensitive to the deviation of κ. This sensitivity study indicates that more accurate measurement of aerosol hygroscopicity properties should be performed, especially for a relatively low supersaturation case. From the results shown in Figure 8, it is also recommended that direct and accurate measurement of large particles' hygroscopicity is necessary since it is them that participate in the droplet formation.

5. Conclusions

In this paper, we have proposed a new method to calculate supersaturation ratio in the ambient activation process using in situ aerosol and droplet measurement data based on the inverse application of κ-Köhler theory. This method combines hygroscopic growth around saturation and activation behavior of aerosol particles together to give insights on the process of ambient activation. In addition to ambient activation process like fogs or clouds, this method can also be applied to other visibility degradation events like haze or mist, and the supersaturation can be assumed both positive and negative corresponding to supersaturation and subsaturation case, respectively.

This newly proposed method was then applied to a fog episode that occurred in the North China Plain, and quite low supersaturations with a maximum of 0.05% are derived. The sensitivity analysis showed that a 10% change of observed droplet number concentrations would result in a supersaturation difference of 0.005%. The lower the ambient water vapor supersaturation, the more errors will arise from the hygroscopic parameter inaccuracy. Activation diameter range in the fog episode obtained through this method suggests that maybe conventional CCN observations should be improved with a lower supersaturation to better depict the aerosol activation properties for low-supersaturation activation case.

The supersaturation derived from this method can be regarded as an effective supersaturation that connects quasi stable conditions of the preactivation and postactivation process. This new method can deepen our understanding of the ambient activation process and the interactions between aerosol particles and droplets. Supersaturation is quite important for models, but currently there are no reliable measurement of this

parameter, especially ambient supersaturation. Our study may help to bridge the gap between models and measurements.

Acknowledgments
This work is supported by the National Natural Science Foundation of China (41590872). The data used can be accessed at https://pan.baidu.com/s/1uovNTxWGMZ8mBUSbyUlVpg. They are also available upon request to the authors.

References

Ackerman, A. S., Kirkpatrick, M. P., Stevens, D. E., & Toon, O. B. (2004). The impact of humidity above stratiform clouds on indirect aerosol climate forcing. *Nature*, *432*(7020), 1014–1017. https://doi.org/10.1038/nature03174

Bott, A., Sievers, U., & Zdunkowski, W. (1990). A radiation fog model with a detailed treatment of the interaction between radiative-transfer and fog microphysics. *Journal of the Atmospheric Sciences*, *47*(18), 2153–2166. https://doi.org/10.1175/1520-0469(1990)047<2153:Arfmwa>2.0.Co;2

Chen, J., Zhao, C. S., Ma, N., Liu, P. F., Göbel, T., Hallbauer, E., et al. (2012). A parameterization of low visibilities for hazy days in the North China Plain. *Atmospheric Chemistry and Physics*, *12*(11), 4935–4950. https://doi.org/10.5194/acp-12-4935-2012

Cheng, C. T., Wang, W. C., & Chen, J. P. (2007). A modelling study of aerosol impacts on cloud microphysics and radiative properties. *Quarterly Journal of the Royal Meteorological Society*, *133*(623), 283–297. https://doi.org/10.1002/qj.25

Deng, Z. Z., Zhao, C. S., Ma, N., Liu, P. F., Ran, L., Xu, W. Y., et al. (2011). Size-resolved and bulk activation properties of aerosols in the North China Plain. *Atmospheric Chemistry and Physics*, *11*(8), 3835–3846. https://doi.org/10.5194/acp-11-3835-2011

Deng, Z. Z., Zhao, C. S., Ma, N., Ran, L., Zhou, G. Q., Lu, D. R., & Zhou, X. J. (2013). An examination of parameterizations for the CCN number concentration based on in situ measurements of aerosol activation properties in the North China Plain. *Atmospheric Chemistry and Physics*, *13*(13), 6227–6237. https://doi.org/10.5194/acp-13-6227-2013

Dusek, U., Reischl, G. P., & Hitzenberger, R. (2006). CCN activation of pure and coated carbon black particles. *Environmental Science & Technology*, *40*(4), 1223–1230. https://doi.org/10.1021/es0503478

Elias, T., Haeffelin, M., Drobinski, P., Gomes, L., Rangognio, J., Bergot, T., et al. (2009). Particulate contribution to extinction of visible radiation: Pollution, haze, and fog. *Atmospheric Research*, *92*(4), 443–454. https://doi.org/10.1016/j.atmosres.2009.01.006

Ervens, B., Cubison, M. J., Andrews, E., Feingold, G., Ogren, J. A., Jimenez, J. L., et al. (2010). CCN predictions using simplified assumptions of organic aerosol composition and mixing state: A synthesis from six different locations. *Atmospheric Chemistry and Physics*, *10*(10), 4795–4807. https://doi.org/10.5194/acp-10-4795-2010

Frank, G., Martinsson, B. G., Cederfelt, S. I., Berg, O. H., Swietlicki, E., Wendisch, M., et al. (1998). Droplet formation and growth in polluted fogs. *Contributions to Atmospheric Physics*, *71*(1), 65–85.

Gerber, H. (1991). Supersaturation and droplet spectral evolution in fog. *Journal of the Atmospheric Sciences*, *48*(24), 2569–2588. https://doi.org/10.1175/1520-0469(1991)048<2569:Sadsei>2.0.Co;2

Gerber, H. E. (1980). A saturation hygrometer for the measurement of relative-humidity between 95-percent and 105-percent. *Journal of Applied Meteorology*, *19*(10), 1196–1208. https://doi.org/10.1175/1520-0450(1980)019<1196:Ashftm>2.0.Co;2

Gerber, H. E. (1981). Microstructure of a radiation fog. *Journal of the Atmospheric Sciences*, *38*(2), 454–458. https://doi.org/10.1175/1520-0469(1981)038<0454:Moarf>2.0.Co;2

Guo, J. P., Su, T. N., Li, Z. Q., Miao, Y. C., Li, J., Liu, H., et al. (2017). Declining frequency of summertime local-scale precipitation over eastern China from 1970 to 2010 and its potential link to aerosols. *Geophysical Research Letters*, *44*, 5700–5708. https://doi.org/10.1002/2017gl073533

Hammer, E., Gysel, M., Roberts, G. C., Elias, T., Hofer, J., Hoyle, C. R., et al. (2014). Size-dependent particle activation properties in fog during the ParisFog 2012/13 field campaign. *Atmospheric Chemistry and Physics*, *14*(19), 10517–10533. https://doi.org/10.5194/acp-14-10517-2014

Hasegawa, S., & Little, J. W. (1977). NBS 2-pressure humidity generator, MARK-2. *Journal of Research of the National Bureau of Standards Section A-Physics and Chemistry*, *81A*(1), 81–88. https://doi.org/10.6028/jres.081A.010

Herich, H., Tritscher, T., Wiacek, A., Gysel, M., Weingartner, E., Lohmann, U., et al. (2009). Water uptake of clay and desert dust aerosol particles at sub- and supersaturated water vapor conditions. *Physical Chemistry Chemical Physics*, *11*(36), 7804–7809. https://doi.org/10.1039/b901585j

Hudson, J. G. (1980). Relationship between fog condensation nuclei and fog microstructure. *Journal of the Atmospheric Sciences*, *37*(8), 1854–1867. https://doi.org/10.1175/1520-0469(1980)037<1854:Rbfcna>2.0.Co;2

Jaatinen, A., Romakkaniemi, J., Anttila, T., Hyvärinen, A.-P., Hao, L. Q., Kortelainen, A., et al. (2014). The third Pallas cloud experiment: Consistency between the aerosol hygroscopic growth and CCN activity. *Boreal Environment Research*, *19*(supplement B), 368–382.

Kiehl, J. T., & Briegleb, B. P. (1993). The relative roles of sulfate aerosols and greenhouse gases in climate forcing. *Science*, *260*(5106), 311–314. https://doi.org/10.1126/science.260.5106.311

Kohler, H. (1936). The nucleus in and the growth of hygroscopic droplets. *Transactions of the Faraday Society*, *32*(0), 1152–1161. https://doi.org/10.1039/tf9363201152

Korolev, A., & Isaac, G. A. (2006). Relative humidity in liquid, mixed-phase, and ice clouds. *Journal of the Atmospheric Sciences*, *63*(11), 2865–2880. https://doi.org/10.1175/Jas3784.1

Kulmala, M., Laaksonen, A., Charlson, R. J., & Korhonen, P. (1997). Clouds without supersaturation. *Nature*, *388*(6640), 336–337. https://doi.org/10.1038/41000

Lamb, D., & Verlinde, J. (2011). *Physics and chemistry of clouds*. New York: Cambridge University Press. https://doi.org/10.1017/CBO9780511976377

Liu, H. J., Zhao, C. S., Nekat, B., Ma, N., Wiedensohler, A., van Pinxteren, D., et al. (2014). Aerosol hygroscopicity derived from size-segregated chemical composition and its parameterization in the North China Plain. *Atmospheric Chemistry and Physics*, *14*(5), 2525–2539. https://doi.org/10.5194/acp-14-2525-2014

Liu, P. F., Zhao, C. S., Gobel, T., Hallbauer, E., Nowak, A., Ran, L., et al. (2011). Hygroscopic properties of aerosol particles at high relative humidity and their diurnal variations in the North China Plain. *Atmospheric Chemistry and Physics*, *11*(7), 3479–3494. https://doi.org/10.5194/acp-11-3479-2011

Ma, N., Zhao, C. S., Nowak, A., Muller, T., Pfeifer, S., Cheng, Y. F., et al. (2011). Aerosol optical properties in the North China Plain during HaChi campaign: An in-situ optical closure study. *Atmospheric Chemistry and Physics*, *11*(12), 5959–5973. https://doi.org/10.5194/acp-11-5959-2011

Mazoyer, M., Burnet, F., Roberts, G. C., Haeffelin, M., Dupont, J. C., & Elias, T. (2016). Experimental study of the aerosol impact on fog microphysics. *Atmospheric Chemistry and Physics Discussions*, 1–35. https://doi.org/10.5194/acp-2016-103

Nan, M. A., Zhao, C., Deng, Z., Tao, J., Renjie, Y. U., Jing, C., & Bian, Y. (2014). A modified method for calibrating the supersaturations in DMT cloud condensation nuclei counter. *Acta Scientiarum Naturalium Universitatis Pekinensis*, *50*(5), 805–811.

Petters, M. D., & Kreidenweis, S. M. (2007). A single parameter representation of hygroscopic growth and cloud condensation nucleus activity. *Atmospheric Chemistry and Physics*, *7*(8), 1961–1971. https://doi.org/10.5194/acp-7-1961-2007

Petters, M. D., Wex, H., Carrico, C. M., Hallbauer, E., Massling, A., McMeeking, G. R., et al. (2009). Towards closing the gap between hygroscopic growth and activation for secondary organic aerosol—Part 2: Theoretical approaches. *Atmospheric Chemistry and Physics*, *9*(12), 3999–4009. https://doi.org/10.5194/acp-9-3999-2009

Prenni, A. J., Petters, M. D., Kreidenweis, S. M., DeMott, P. J., & Ziemann, P. J. (2007). Cloud droplet activation of secondary organic aerosol. *Journal of Geophysical Research*, *112*, D10223. https://doi.org/10.1029/2006JD007963

Pruppacher, H. R., & Klett, J. D. (2004). *Microphysics of clouds and precipitation*. New York: Kluwer Academic.

Ran, L., Zhao, C. S., Xu, W. Y., Lu, X. Q., Han, M., Lin, W. L., et al. (2011). VOC reactivity and its effect on ozone production during the HaChi summer campaign. *Atmospheric Chemistry and Physics*, *11*(10), 4657–4667. https://doi.org/10.5194/acp-11-4657-2011

Ren, J., Zhang, F., Wang, Y., Collins, D., Fan, X., Jin, X., et al. (2018). Using different assumptions of aerosol mixing state and chemical composition to predict CCN concentrations based on field measurements in urban Beijing. *Atmospheric Chemistry and Physics*, *18*(9), 6907–6921. https://doi.org/10.5194/acp-18-6907-2018

Roach, W. T. (1976). Effect of radiative exchange on growth by condensation of a cloud or fog droplet. *Quarterly Journal of the Royal Meteorological Society*, *102*(432), 361–372. https://doi.org/10.1002/qj.49710243207

Shen, X. J., Sun, J. Y., Zhang, X. Y., Zhang, Y. M., Zhang, L., Che, H. C., et al. (2015). Characterization of submicron aerosols and effect on visibility during a severe haze-fog episode in Yangtze River Delta, China. *Atmospheric Environment*, *120*, 307–316. https://doi.org/10.1016/j.atmosenv.2015.09.011

Spiegel, J. K., Zieger, P., Bukowiecki, N., Hammer, E., Weingartner, E., & Eugster, W. (2012). Evaluating the capabilities and uncertainties of droplet measurements for the fog droplet spectrometer (FM-100). *Atmospheric Measurement Techniques*, *5*(9), 2237–2260. https://doi.org/10.5194/amt-5-2237-2012

Su, T., Li, Z., & Kahn, R. (2018). Relationships between the planetary boundary layer height and surface pollutants derived from lidar observations over China. *Atmospheric Chemistry and Physics Discussions*, *2018*, 1–38. https://doi.org/10.5194/acp-2018-279

Su, T. N., Li, J., Li, J., Li, C. C., Chu, Y. Q., Zhao, Y. M., et al. (2017). The evolution of springtime water vapor over Beijing observed by a high dynamic Raman Lidar system: Case studies. *Ieee Journal of Selected Topics in Applied Earth Observations and Remote Sensing*, *10*(5), 1715–1726. https://doi.org/10.1109/jstars.2017.2653811

Twohy, C. H., & Anderson, J. R. (2008). Droplet nuclei in non-precipitating clouds: Composition and size matter. *Environmental Research Letters*, *3*(4), 045002. https://doi.org/10.1088/1748-9326/3/4/045002

Twomey, S. (1966). Computations of rain formation by coalescence. *Journal of the Atmospheric Sciences*, *23*(4), 405–411. https://doi.org/10.1175/1520-0469(1966)023<0405:Corfbc>2.0.Co;2

Zhang, F., Wang, Y. Y., Peng, J. F., Ren, J. Y., Collins, D., Zhang, R. Y., et al. (2017). Uncertainty in predicting CCN activity of aged and primary aerosols. *Journal of Geophysical Research: Atmospheres*, *122*, 11,723–11,736. https://doi.org/10.1002/2017JD027058